

Analysis of multicomponent walkaway vertical seismic profile data

Bona Wu, Don C. Lawton, and Kevin W. Hall

ABSTRACT

A multicomponent walkaway VSP data processed for PP and PS imaging as well to study the AVO response. To date, a PP wave corridor stack and VSP-CDP mapping have been completed and are correlated to synthetic seismograms. Overall, we saw a good correlation between VSP and synthetic data, and observed changes inside the reservoir, interpreted to be due to production. A common shot stack reflectivity gather was produced for AVO analysis. At the top and bottom of the target reservoir, the AVO responses of VSP PP wave data and synthetic gathers show similar trends. The results give us promise for inverting walkaway VSP data for reservoir properties.

INTRODUCTION

A vertical seismic profile (VSP) is a measurement in which the seismic waves are recorded by geophones secured in a borehole for a seismic source at the surface of the earth. Due to its geometry, a VSP survey is used principally to calibrate surface seismic data by giving an accurate depth-time measurement to geological features. VSP data has greater resolution than surface seismic data and provides more detailed image around the borehole. Although the quality of VSP image decreases dramatically with increase of distance from the borehole, this drawback can be compensated by walkaway VSP. Besides broader frequency bandwidth, VSP survey has other advantages for AVO analysis (Coulombe et al., 1996):(1) VSP data has less noise interference due to the quiet borehole environment, that is the S/N is higher than that of surface seismic data; (2) downgoing wavefield is also recorded and can be used to design the deconvolution operator. This deterministic deconvolution can better remove the wavefield propagation effects such as multiples; (3) a good estimate of the reflection coefficient from VSP is relatively easy to obtain. Considering all these advantages, the walkaway VSP is especially suited for AVO analysis.

The application of converted seismic wave exploration enhances traditional compressional wave exploration in many aspects such as improve reservoir description especially for fluid-contact detection, pore-fluid discrimination and give a more robust way to derive rock properties. The benefits of the converted-wave data in exploration led the processing and interpretation techniques have been developed quickly in the industry.

In this research, a multicomponent walkaway VSP data was used to undertake AVO analysis of the target reservoir. The combination of advantages of VSP and converted - wave data makes the characterization of target reservoir more reliable and the results can be used to guide field development.

3C VSP DATA PROCESSING

Both zero-offset and far-offset shots were processed to corridor stack and VSP-CDP mapping stages, respectively, and tied to nearby well logs. Also, both P-P and P-S

reflections were converted to depth domain through prestack depth migration. The VISTA software from GEDCO was used for the data processing.

Data acquisition

The University of Calgary Envirovibe provided the energy source for a walk-away vertical seismic profile (VSP), in addition to dynamite, at the same source location. The main acquisition parameters of both vibroseis and dynamite surveys are shown in Table 1.

Table 1. Main acquisition parameters for walkaway VSP.

	Dynamite	Vibroseis
Charge (kg)/ Sweep	0.125kg at 9m depth	10-300Hz over 20s, linear, one sweep per vibrate point, 100/1000ms taper
Number of Shots	14	14
Receivers type	VectorSeis	VectorSeis
Number of receivers	220	220
Receiver spacing (m)	2	2
Receiver depth (m)	55-507	55-507
Sample rate (ms)	1	1
Record length (s)	3	3
Offset (m)	11.5-1031	11.5-1031
Source elevation (m)	612-622	612-622
Borehole	562 m TD, Vertical, no fluids in borehole	

Geometry setup and pre-processing of the VSP data

The setup of VSP trace headers and geometry was the first step in processing. The total vertical depth (TVD) was calculated from measured receiver depth and datum or kelly bushing (KB) elevation. In this case, the datum was set at 620 m. The geometry of the walkaway VSP survey is shown in FIG. 1. There were 14 shots recorded for both vibroseis and dynamite surveys respectively and each shot was processed separately. The first arrival was picked on vertical component (*Z*) and the picked values were transferred to the *X* and *Y* components. Some traces with abnormal amplitudes were killed and polarity reversals were corrected.

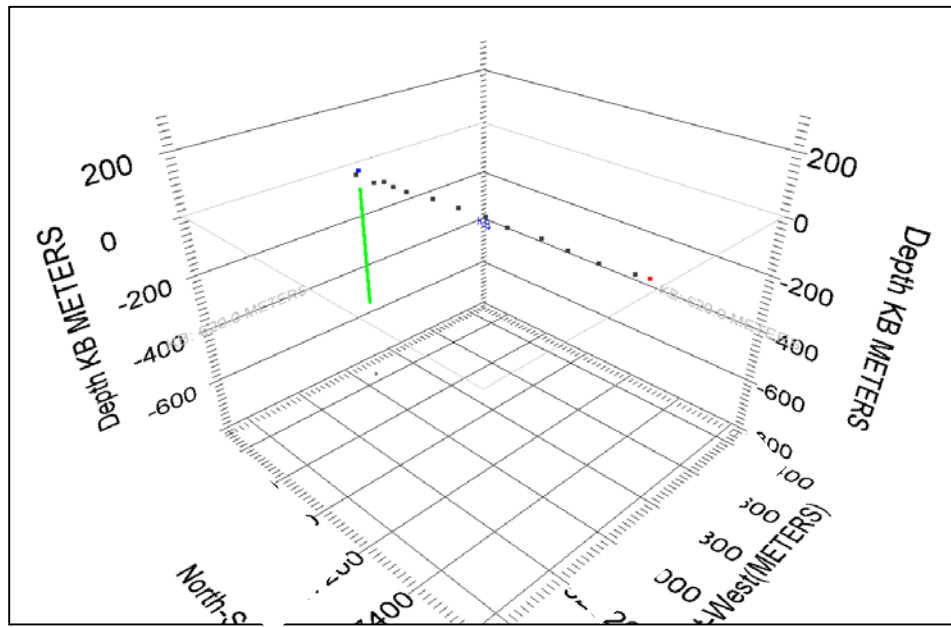


FIG. 1. 3D Geometry of the multicomponent VSP data. Vertical green line is receivers in the borehole, small dots are shot locations.

The dense receiver sampling (2 m) allows many wave modes to be recorded. The vertical component of the Envirovibe zero-offset shot is shown in FIG. 2. Downgoing P primary (yellow), upgoing P (purple), downgoing S (blue), and downgoing P multiple (orange) are identified on the raw record. Similar wave types are shown by the vertical component of a far-offset (153 m) VSP shot (FIG. 3). It is distinct that the S wave is much stronger on the far-offset shot than on the zero-offset shot due to the incident angle change. Furthermore, higher amplitude downgoing shear wave shows on Vibroseis shot records because that Envirovibe source generates a stronger direct downgoing shear wave than the dynamite source (Hall et al., 2012). It is more visible on the radial component record (FIG. 4).

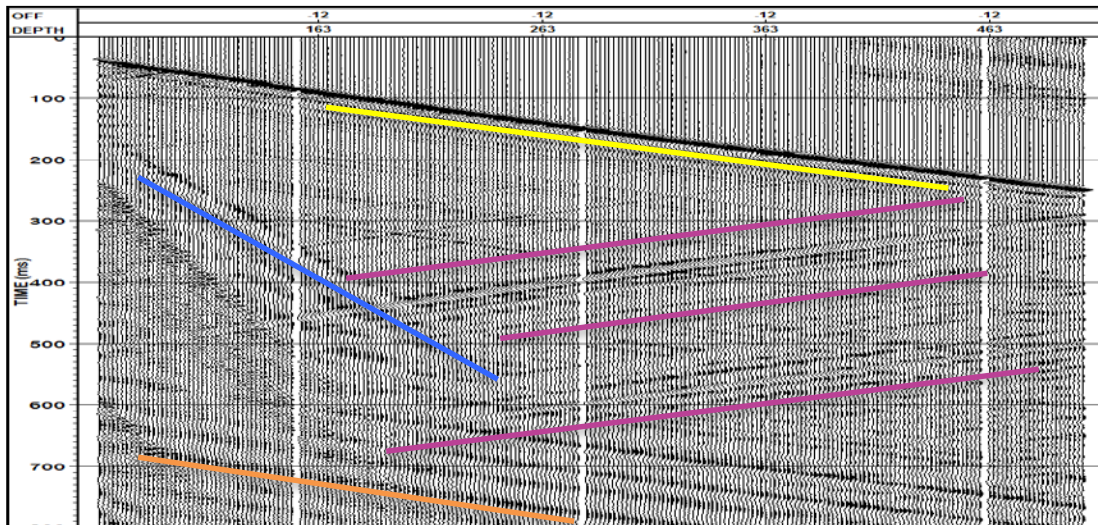


FIG. 2. Vertical component of vibroseis zero-offset shot: downgoing P primary (yellow), upgoing P (purple), downgoing shear (blue), and downgoing P multiple (orange) waves (display with AGC=200 ms).

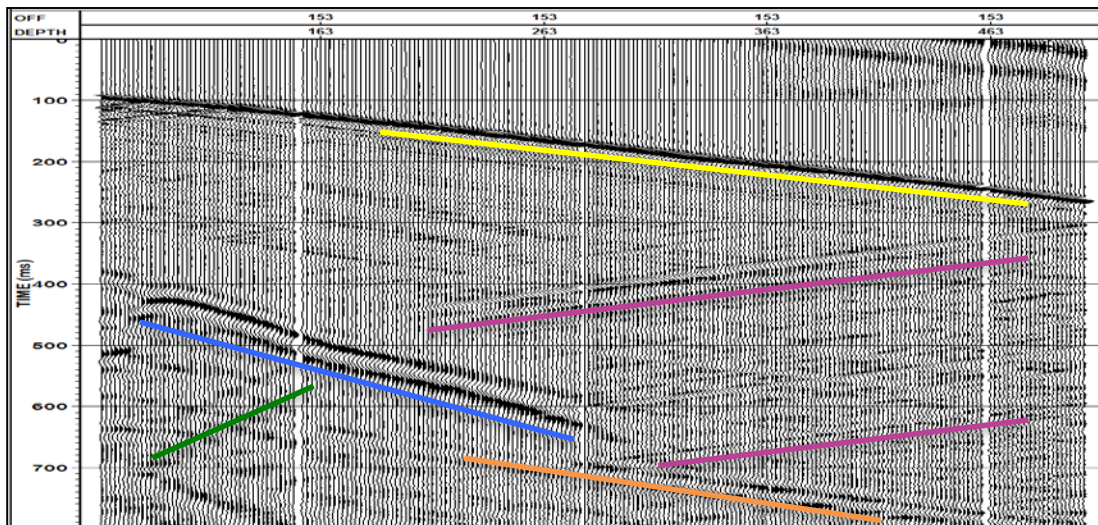


FIG. 3. Vertical component of vibroseis offset shot (offset=153 m): downgoing P (yellow), upgoing P (purple), downgoing S (blue), upgoing S (green), and downgoing P multiple (orange) waves (display with AGC=200 ms).

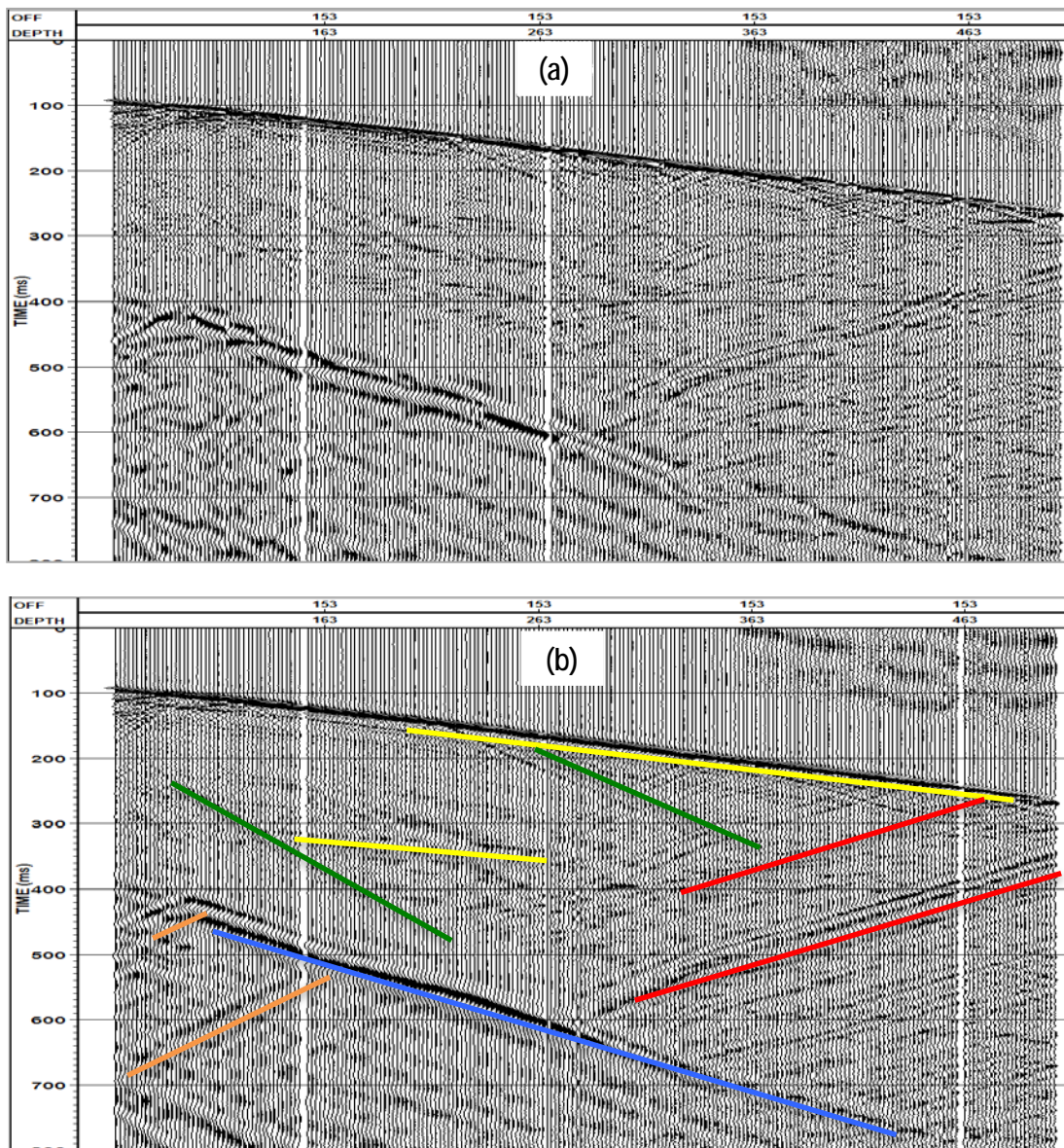


FIG. 4. Horizontal component of vibroseis offset shot (offset=153 m) (a) before and (b) after horizontal rotation (display with AGC=200 ms). Downgoing P is marked by yellow line, downgoing SV (direct arrival) is marked by blue line, transmitted downgoing S is marked by green line (converted from downgoing P), upgoing SV (converted from downgoing P) is marked by red line, and reflected SV wave (SS) is marked by the orange line.

Compared with vertical component, the horizontal component Hmax (after rotation) is dominated by shear waves and the wavefield is more complex. The yellow line marked downgoing P, blue line marked downgoing SV and green line marked the converted S from downgoing P. The upgoing SV (converted PS) is marked by red line and the reflected SV wave (SS) is marked by orange line.

VSP data processing flow

After preprocessing, the zero-offset and far-offset VSP data were processed separately using different processing workflows. FIG. 5 shows the flow charts of both zero-offset

and far-offset VSP data processing. The details of processing parameters and results are discussed in the following section.

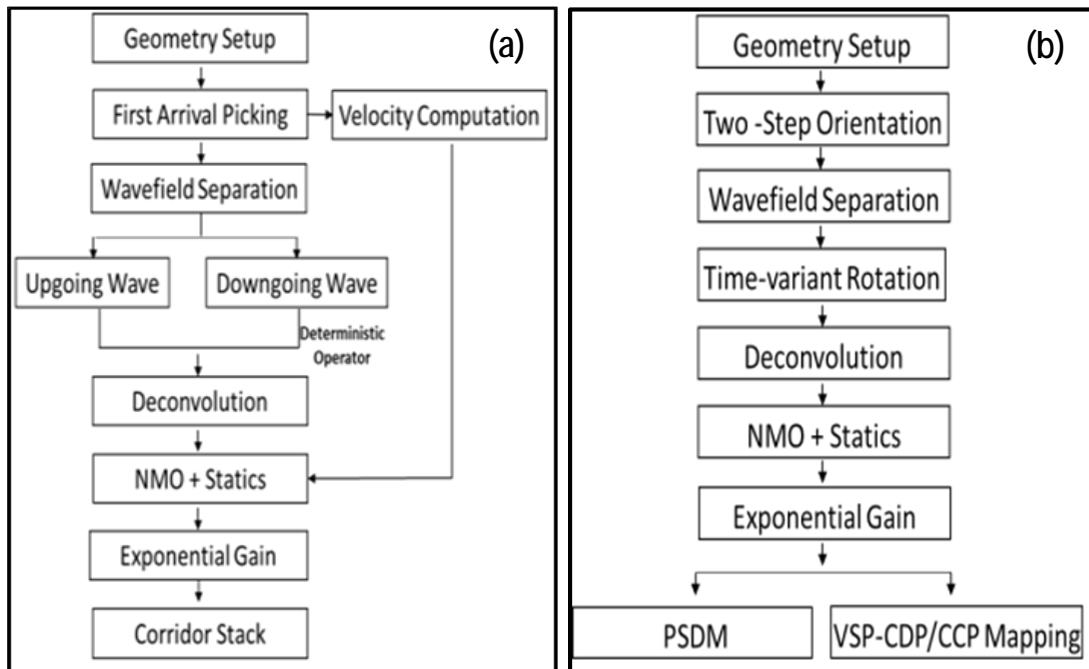


FIG. 5. Zero-offset (a) and far-offset (b) VSP processing sequences

Zero-offset VSP processing

The interval velocity profile was calculated from first arrival time of zero-offset VSP data and is shown in FIG. 6. Any anomalies of the velocity were recomputed after correcting the first arrival picking time or were deleted. The velocity range is from 1700 to 2500 m/s. It was used for NMO correction, time-variant polarization of far-offset VSP and calibration of sonic logs, discussed in detail later.

First arrivals were flattened to an arbitrary time to align downgoing waves. Then median filtering was used to separate downgoing and upgoing wavefield. Different filter lengths (number of traces) were tested. The test results indicated that longer filter worked better to separate upgoing waves from downgoing waves. Thus, a 19-trace median filter was chosen for the wavefield separation. Downgoing multiples can be easily spotted on downgoing waves; they need to be attenuated by deconvolution in the subsequent processing.

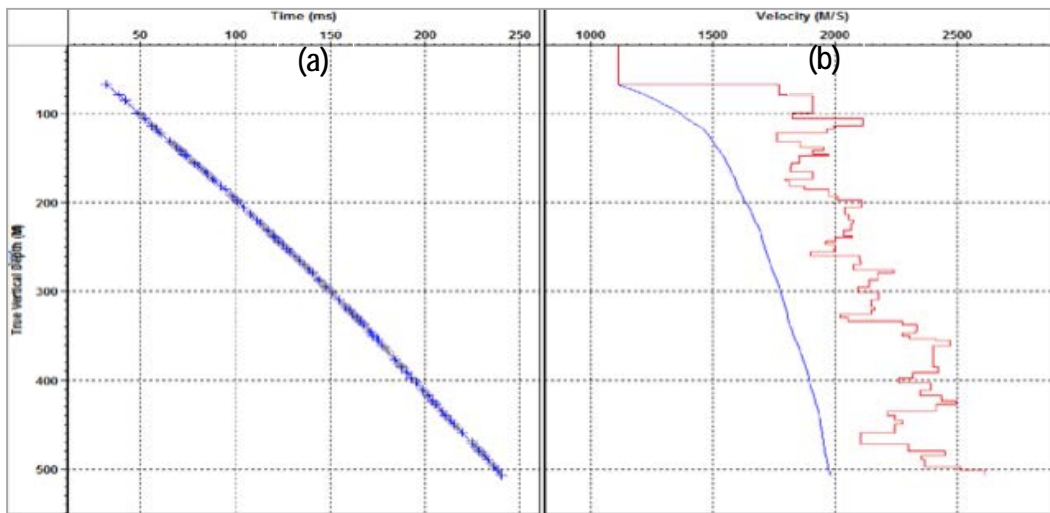


FIG. 6. Velocity profile calculated from first arrival time of zero-offset VSP data. (a) the picks for velocity profile are marked in blue, bad picks are marked in grey. (b) blue curve is the RMS velocity and the red curve is the calculated interval velocities.

A deconvolution operator was designed on the downgoing wave within a window of -50ms to +250ms from first arrival time. Based on tests, a 300 ms operator with 5% pre-whitening were applied. After deconvolution, the downgoing multiples were greatly suppressed and frequency spectra were whitened. Furthermore, the signal-to-noise ratio was also enhanced by deconvolution (from 20 db to 100 db on average). This operator was then applied to the upgoing wavefield. Both sharpness of events and signal-to-noise ratio were improved (FIG. 7). Ideally, the deconvolution also corrected output data to zero phase automatically.

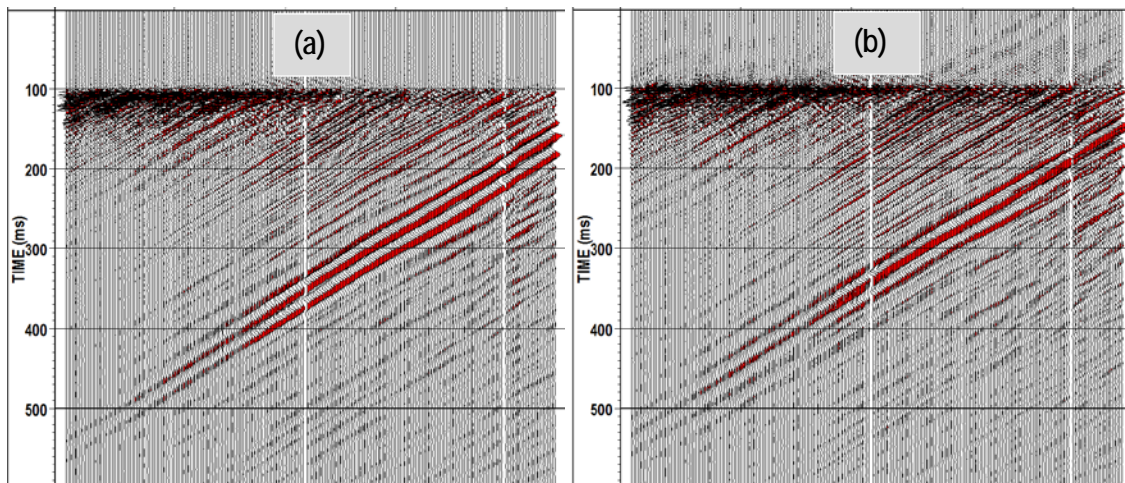


FIG. 7. Upgoing P wave of a dynamite shot before (a) and after (b) deconvolution.

Amplitude loss was recovered by two procedures: 1) an amplitude scalar was calculated from the downgoing wave (window= ± 10 ms from first break time) and applied on upgoing waves to compensate amplitude loss along the downgoing wave travel path; 2) exponential gain was then applied to account for amplitude loss (absorption as well)

along upgoing wave paths. In this study, parameter 1.6 was used to calculate gain value from first arrival time. After the processing, the amplitude is balanced over shallow and deep depth and time.

NMO correction and statics were then applied on the upgoing waves before corridor stack. Shot statics were provided. After application of NMO and statics, all the reflections were flattened so that they could be stacked constructively.

Although noise attenuation was implemented with a 5-trace median filter, SV wave contamination and residual multiples still present. Since multiples are outside of the defined corridor, they will not degrade the corridor stack. In this study, a 30 ms corridor mute was applied based on the data. The gather before and after corridor mute and stacks are shown in FIG. 8 and FIG. 9, respectively. Comparing with full stacks, apparently, without contamination of multiples, corridor stack has higher resolution and signal to noise ratio than full stack.

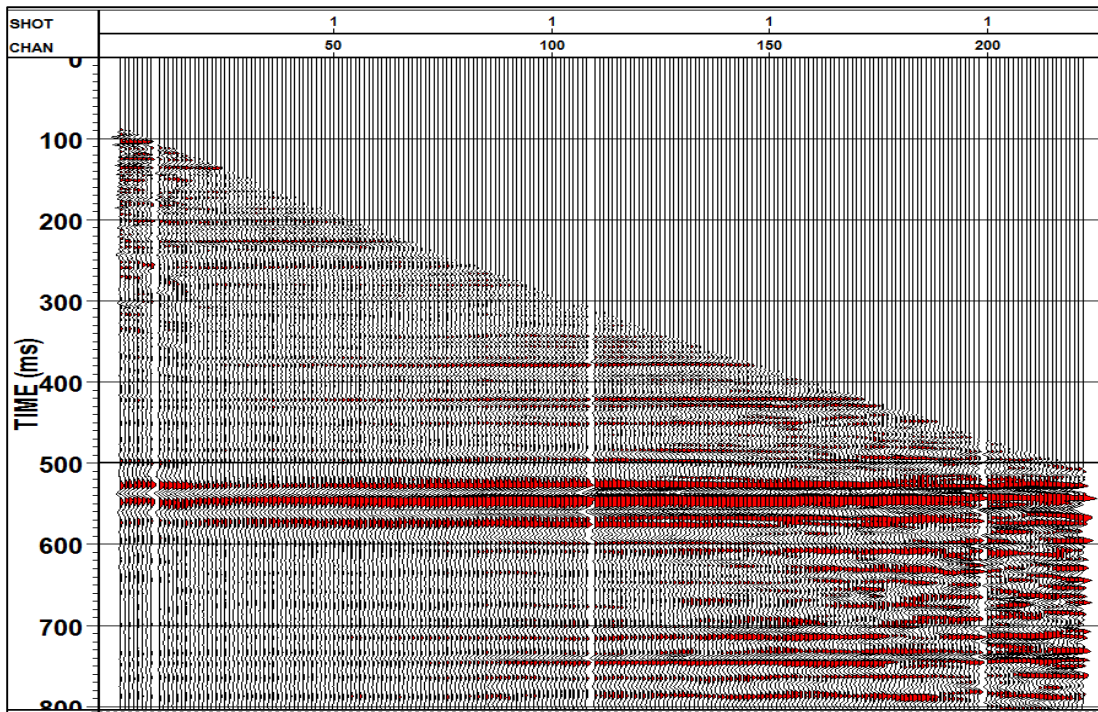


FIG. 8. +TT plot of processed upgoing wave gather of dynamite zero offset shot (vertical component)

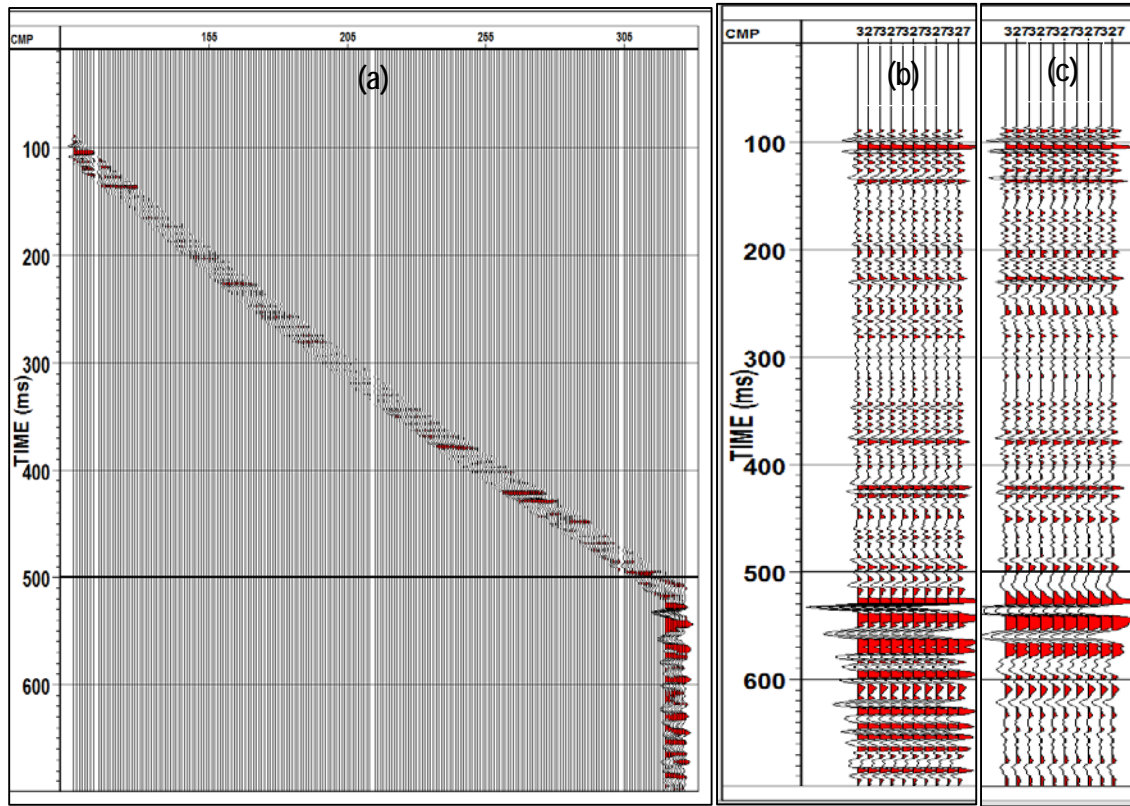


FIG. 9. Dynamite zero offset shot (vertical component). (a) upgoing wave gather after corridor mute; (b) corridor stack (repeated 10 times); (c) full stack (repeated 10 times).

Far-offset VSP processing

During preprocessing, the X and Y were already rotated into Hmax and Hmin. However, various wave types still appear on both horizontal and vertical components. Especially, it is not possible to separate downgoing P from any single component, which is important for deconvolution operator design and amplitude scaling. So a second rotation is required to transform the vertical component (Z) and Hmax into Hmax' and Z'. Hmax' is toward the source direction and Z' is perpendicular to it. FIG. 10 shows the hodogram analysis of the second rotation. It was seen that the rotation angle (angle between horizontal and source-receiver direction) increases with depth due to VSP geometry (red bars on FIG. 10). After rotation, it is assumed only downgoing P and upgoing SV energy on Hmax', and upgoing P and downgoing SV waves dominates Z'. Although the real data contains other types of modes, these assumptions benefit the subsequent wavefield separation and other processing.

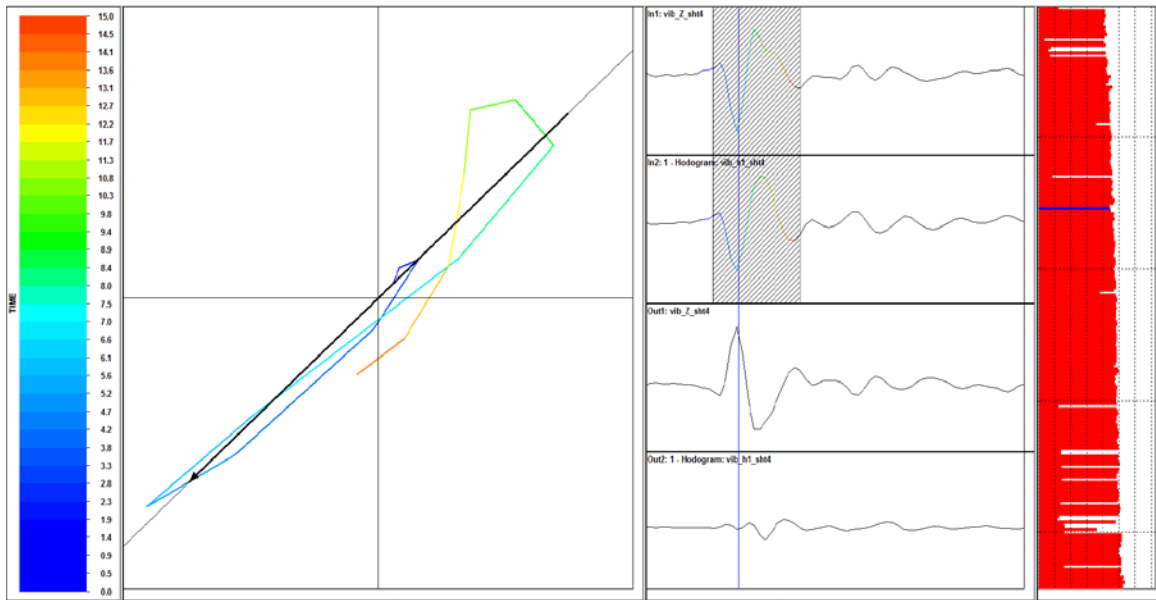


FIG. 10. The hodogram analysis between Vertical and Hmax components of shot 4 (offset=153m, channel=270). The red bars on the right are rotation angles which increase along the depth.

Similar to zero-offset VSP processing, first arrivals were flattened to arbitrary times to align downgoing waves of Hmax' and Z' components. Then a median filter was used to separate downgoing and upgoing wavefield. Different filter lengths (from 11 to 19 traces) were tested and the optimized 15 trace median filter was applied for this shot.

However, the wavefield separation of far-offset VSP is complicated due to its geometry. The incident angles decrease with increasing depth of geophones, and also, the polarization angles change with time. So time-variant polarization is required to achieve wavefield separation for far-offset VSP. In practice, the upgoing waves were separated from Z' and Hmax' and rotated back to original Z and Hmax directions. Then the upgoing P and SV waves were separated through time-variant polarization based on ray tracing method using the velocity model from zero-offset VSP data. The velocity model and ray tracing is shown in FIG. 11. However, some downgoing waves are also present on both components since it is difficult to remove them by median filter only when isolating the upgoing waves. They were removed by application of an FK filter before VSP-CDP mapping.

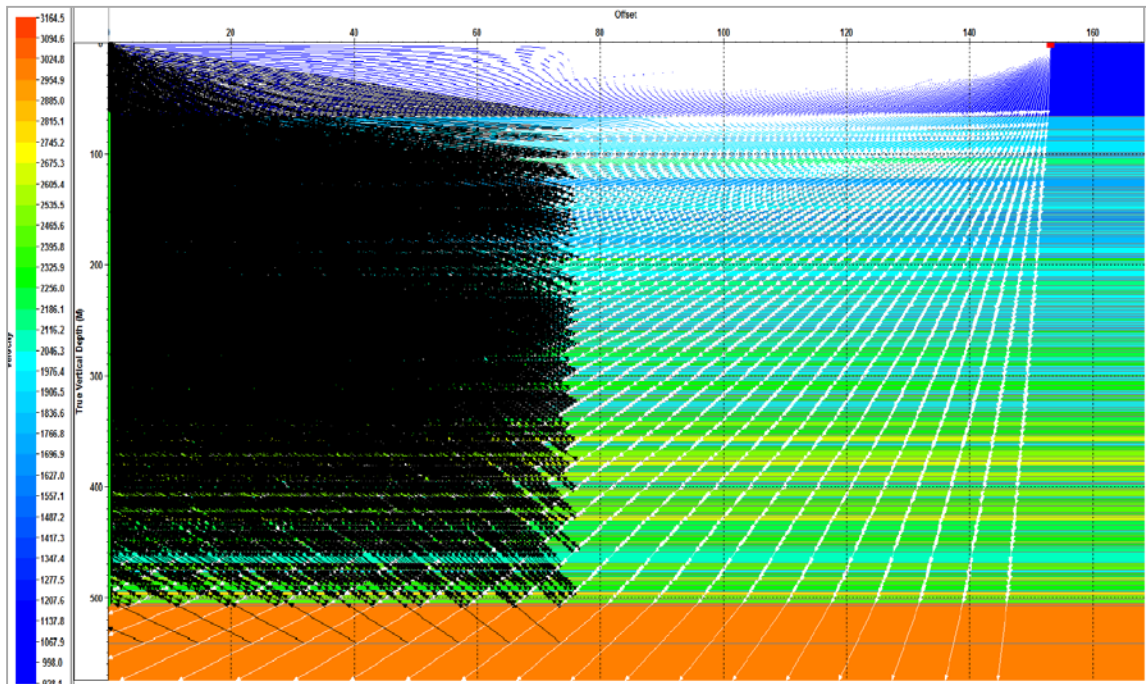


FIG. 11. Ray tracing of the subsurface model (200 rays was used for demonstration, 2000 rays was used for actual processing). White lines are downgoing rays and black lines are reflected upgoing waves.

Since there is no shear wave velocity from well log, the shear wave velocity was obtained by a velocity scan method. After upgoing P and SV waves were isolated by time-variant polarization, deterministic deconvolution was applied to them.

A few processing techniques were then applied to upgoing waves before VSP-CDP or VSP-CCP mapping. They are exponential gain, VSP NMO, SV event attenuation by FK filter, and noise attenuation, by 5-trace median filter and band-pass filter. Considering relatively small receiver interval (2 m), a 2 m bin size was chosen for the P wave and PS data. FIG. 12 shows the VSP-CDP mapping of dynamite and Vibroseis shots. With phase correction in the processing, both types of sources give comparable images but the dynamite data shows a slightly higher resolution.

FIG. 13 shows the P wave velocity model for the pre-stack depth migration (PSDM). For the P-S PSDM, a constant V_p/V_s ratio of 2.5 was applied. The migrated image of a dynamite shot was shown in FIG. 14. Due to a limited aperture, the VSP migration image (90° dip limit) always shows strong artifacts. Both PP and PS images show similar characteristics of major reflections but it is clear that the PS image gives higher resolution. In theory, when PS events were recorded near their point of origin (the conversion point), they have the same temporal frequency as P-waves. Because of this, the PS events often have significantly higher resolution or shorter wavelengths than P-waves (Lawton et al., 2012). The difference brings great difficulty for PP-PS registration.

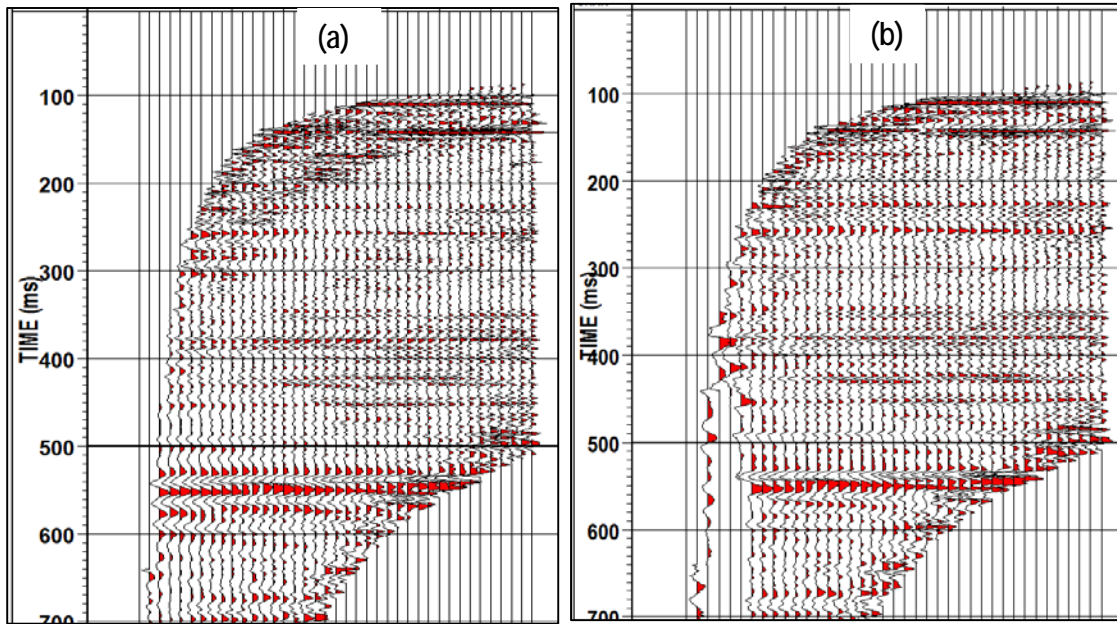


FIG. 12. (a) Dynamite vs (b) vibroseis VSP - CDP mapping of upgoing P wave of shot 4 (offset=153m). Resampled grid size=2 m. (AGC=200 ms was applied for display)

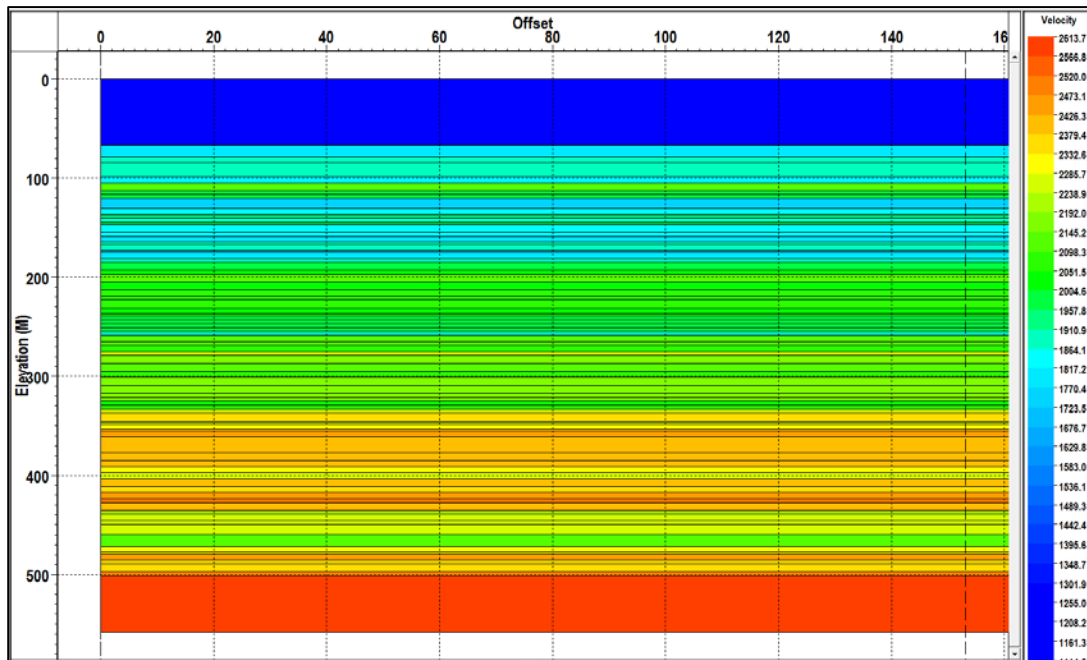


FIG. 13. P wave velocity model for PSDM. Velocities units are in m/s.

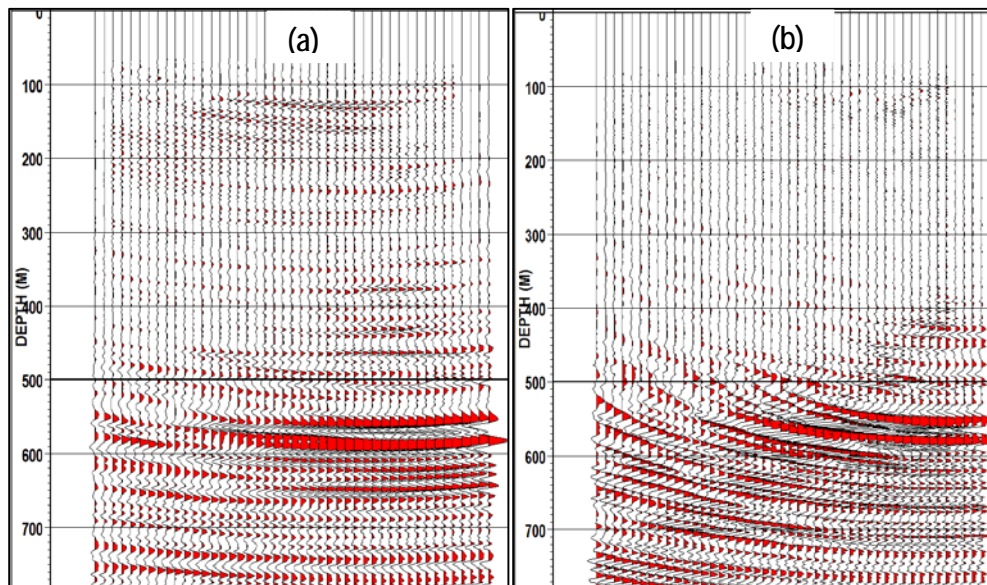


FIG. 14. PSDM of (a) upgoing P and (b) upgoing S waves of a dynamite shot (offset=214 m). Constant $V_p/V_s=2.5$ was used in PS-PSDM and it shows higher resolution than PP data.

AVO ANALYSIS

Calibration of well logs

P-wave sonic and density data from a nearby well (about 200 m away) are available in this area. Due to the difference in measurement frequency, sonic logs generally yield higher velocities than those from VSP data. Cumulatively, VSP one-wave P wave travel time is about 8 ms longer than that calculated from sonic log. In order to tie synthetic seismograms to VSP data, the well logs were firstly calibrated with VSP velocity. The calibration of sonic log is shown in FIG. 15. After calibration, the drift between aforementioned two one-way P wave travel times was reduced to ± 0.2 ms.

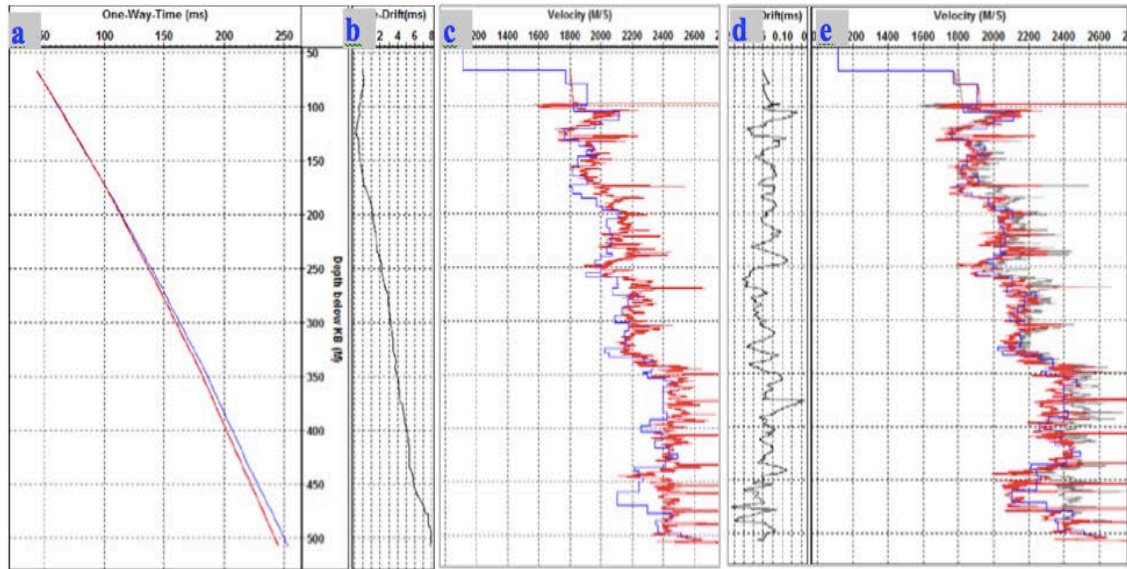


FIG. 15. Sonic log calibration: (a) time-depth curves, VSP one-way P time in blue, sonic log calculated one-way P wave time in red, (b) time drift between VSP and well log before calibration, (c) comparison of VSP (blue) and sonic log (red) interval velocities before calibration (d) time drift after calibration, (e) comparison of VSP (blue) and sonic log (red) interval velocities after calibration. The original sonic logs are plotted in grey.

Zero offset P wave synthetic seismogram

The zero offset PP synthetic seismogram was generated by GeoSyn software. FIG. 16 shows the wavelet extracted from VSP corridor stack, as used to create the synthetic seismogram. FIG. 17 shows the correlation between the synthetic seismogram and corridor stack. The synthetic seismogram with 90° phase shift and reverse polarity display gives best correlation with the corridor stack. Major formations in this area are marked on the corridor stack and most of them show good match to the synthetic seismogram. Reflections from the reservoir show obvious amplitude and phase differences from the synthetic seismogram. The distance between the logging well and VSP borehole makes the correlation less reliable. It is also possibly caused by the fluid changes of the reservoir because of production since the well log was attained.

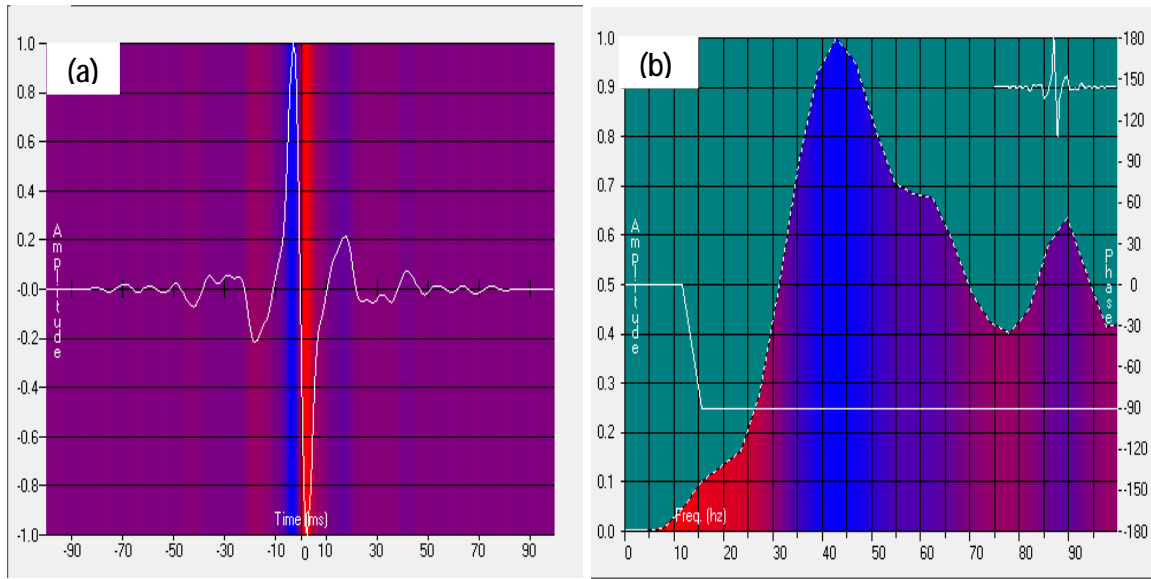


FIG. 16. (a) the wavelet extracted from corridor stack (after 90° phase shift, operator length=200 ms); (b) spectrum of the wavelet.

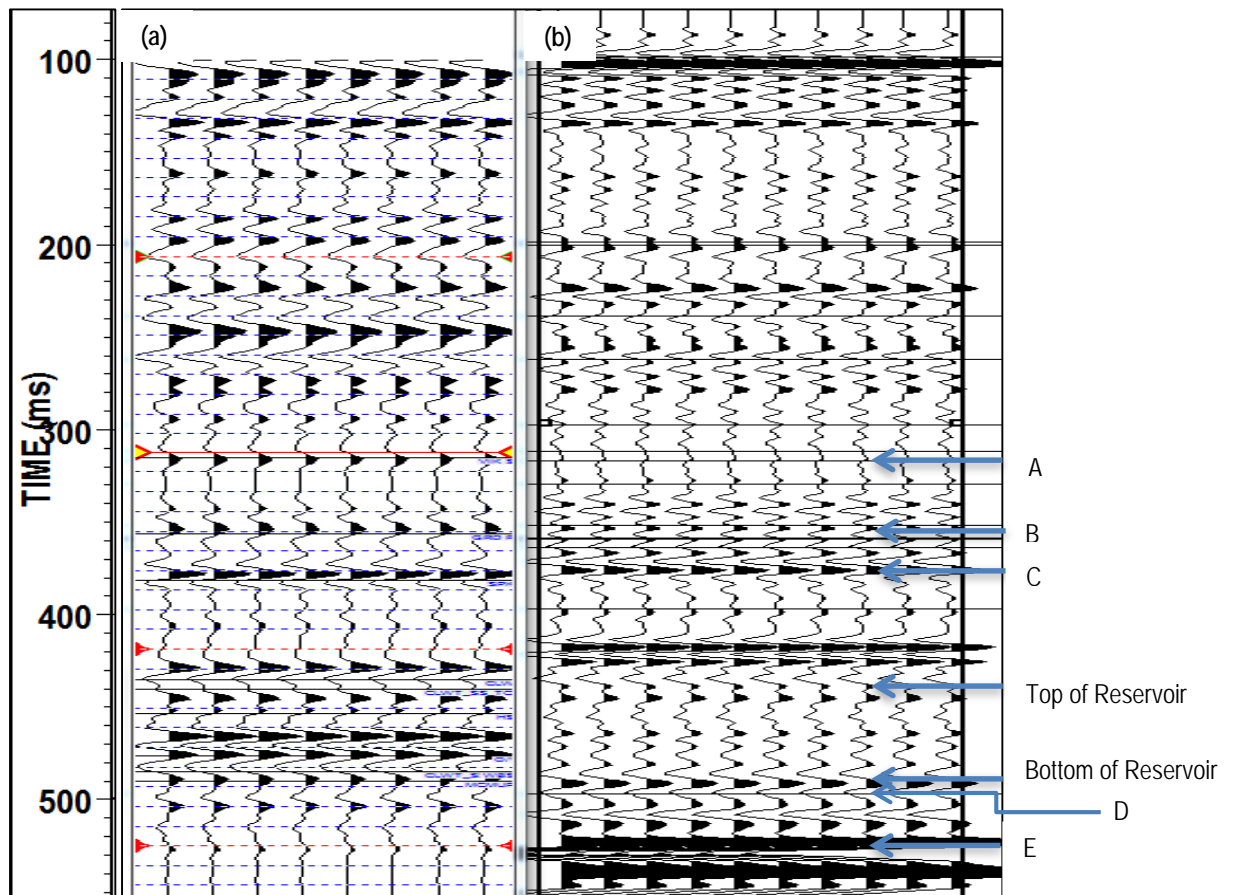


FIG. 17. Correlation of (a) zero-offset PP synthetic seismogram and (b) VSP corridor stack.

Offset P wave synthetic seismogram

An offset synthetic offset gather was created using CREWES software SYNGRAM. A 10-150 hz zero phase band-pass filter wavelet was used based on frequency content of VSP data. The comparison of frequency content of processed VSP data to the input wavelet is shown in FIG. 18. The sonic log was blocked to 2 ms considering seismic wave and well log scale difference.

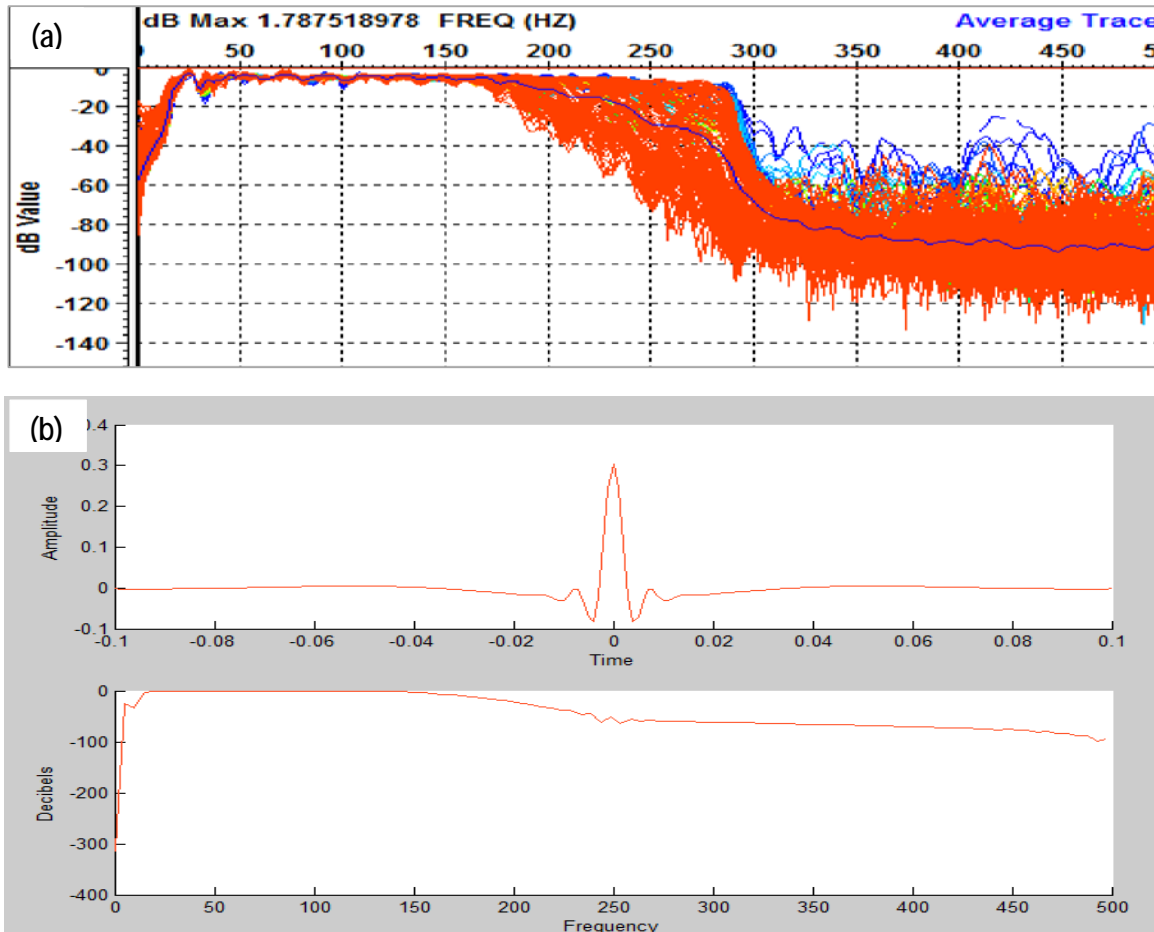


FIG. 18. (a) frequency analysis of upgoing P wave after deconvolution. (b) the band pass filter wavelet used in offset synthetic gather creation and its frequency spectrum.

The composite plots (FIG. 19) show detailed correlation between sonic logs, VSP-CDP mapping of upgoing P wave of a far-offset VSP shot (dynamite, offset=153 m), processed upgoing P (PP) gather and stack traces of zero-offset VSP, and synthetic seismogram of PP wave. Overall, a reasonable correlation of the VSP to the synthetic seismogram was observed. However, some reflections within the reservoir on synthetic seismograms are not clear on VSP data. The reason is that thin high velocity layers yield strong reflections on synthetic seismic, but might be too thin to be resolved by seismic waves of VSP. Also, due to the small change of the P wave velocity and porosity, the impedances of the interfaces inside the reservoir are too small to be identified on VSP data.

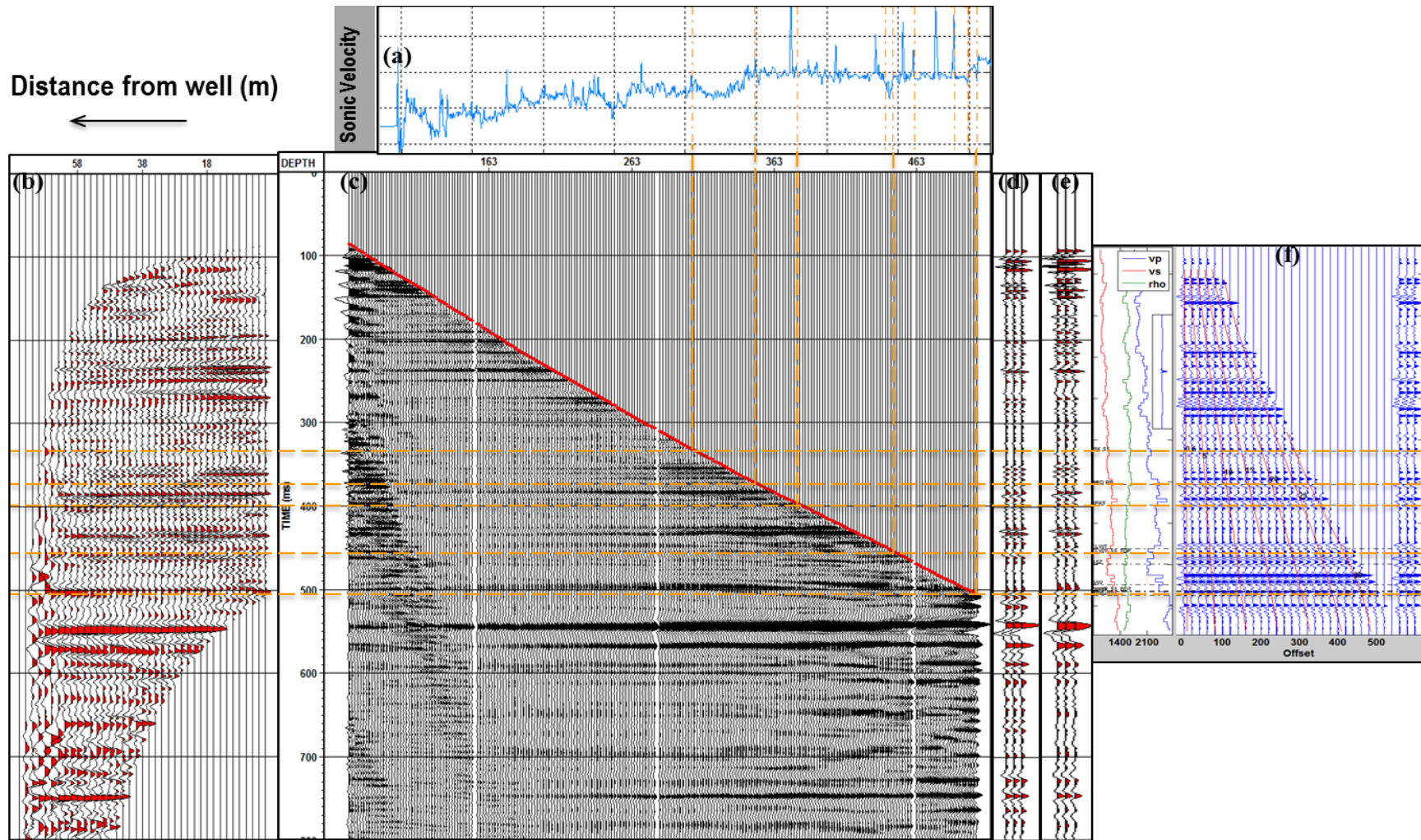


FIG. 19 Composite plot of sonic log, VSP data and synthetic seismogram. (a) sonic log, (b) VSP-CDP mapping of upgoing P of a far-offset VSP (offset=153 m), (c) processed upgoing P wave gather of zero-offset VSP, (d) corridor stack, (e) non-corridor stack, (f) synthetic offset gather and its stack trace (repeated 3 times).

AVO analysis of a VSP reflectivity

The well logs from nearby well give more details about the target reservoir, as shown in FIG. 20. In the reservoir and transition zones, the GR is relatively low which indicates clean sand deposits. High porosity in these zones indicates a good hydrocarbon reservoir. Also, the sonic velocity is slightly higher than the overlying shale while the density is relatively low in the reservoir. The core in this interval shows that top of the reservoir is dominated by tidal-fluvial channel faces, while the middle and bottom of the reservoir are dominated by sand flat facies. The deposition and facies analysis will be used to instruct the AVO analysis and further lithology prediction in the target reservoir.

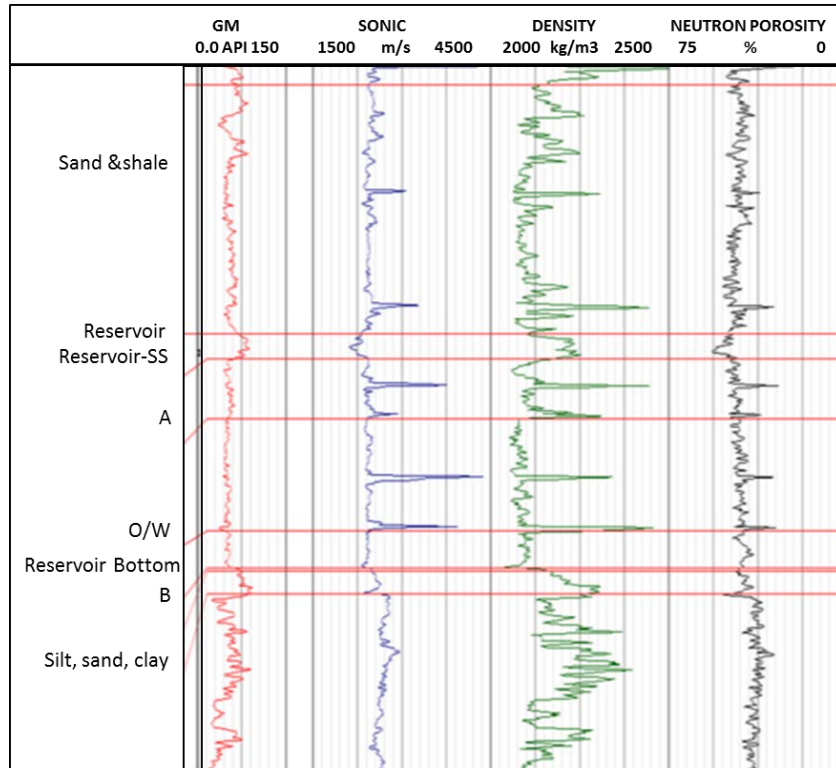


FIG. 20. Well logs from well A. The log curves from left to right are: GM, sonic velocity, density and neutron porosity.

After applying the scalar calculated from downgoing waves, a reflectivity shot gather was created by dividing the upgoing wave amplitude by the downgoing wave amplitude. Then a common shot stack was produced. In order to improve the signal to noise ratio and more accurate reflectivity, a corridor mute (30 ms window) was applied to the shot gather before stack. When all the stacked shot traces were merged together, an offset reflectivity gather was obtained for AVO analysis. FIG. 21 shows the tie of the common shot stack to the synthetic seismogram. Five horizons in the target reservoir were marked on the synthetic seismogram; however, only the top and bottom of the reservoir can be picked correspondingly on VSP data. Inside the reservoir, the amplitude and phases of the VSP data show large differences from synthetic seismogram. There are three possible reasons for the difference: (1) the logged well is 200 m away from VSP borehole, the lithology of the fluvial channel deposit system may change greatly in this distance; (2) the study zone is currently under production, so the properties of reservoir could change

during production; (3) the whole reservoir interval is about 50-75 m and 5 horizons were picked on the well log of this reservoir. Limitation of VSP resolution makes picking seismic horizons within the small time interval challenging.

The amplitudes picked from VSP gather and their offsets are shown in Table 2. FIG. 22 is the amplitude plot of the picked horizons. They both show a decreasing amplitude trend with increasing offset.

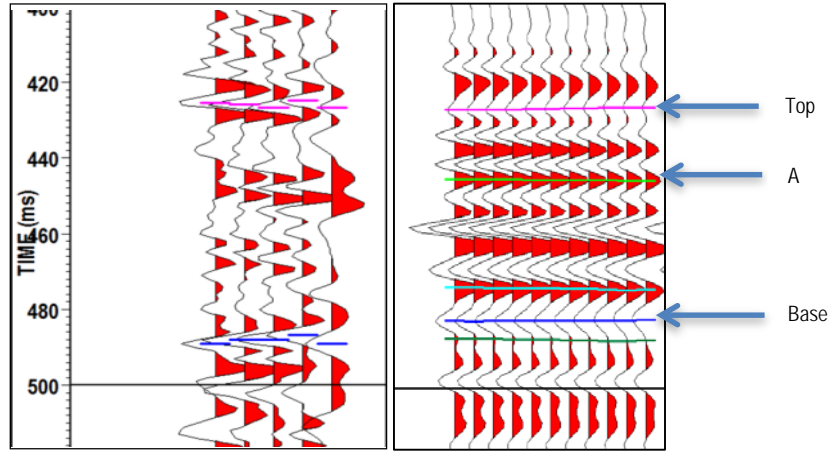


FIG. 21. Correlation between common shot stacks (receiver-offset gather) and synthetic offset gather. Picked horizons from top to bottom are: Top reservoir, Horizon B, Bottom of reservoir.

Table 2. Amplitude picked from VSP gather in the target reservoir.

	OFFSET(m)	SCALED OFFSET	TOP	BASE
Shot1	11.5	23	-0.019	-0.018
Shot3	104	208	-0.019	-0.022
Shot4	153	306	-0.013	-0.020
Shot5	214	428	-0.012	-0.019
Shot6	308	616	-0.006	-0.014

FIG. 23 is the P-P wave synthetic CMP gather and stack (repeated 3 times). Contours show the incident angles and the yellow rectangle marks the target reservoir. A few horizons marked in FIG. 21 are picked on the synthetic seismogram and the values are in Table 3. Plot of this amplitude is shown in FIG. 24. For the picked horizons, the absolute amplitudes all slowly decrease with offset.

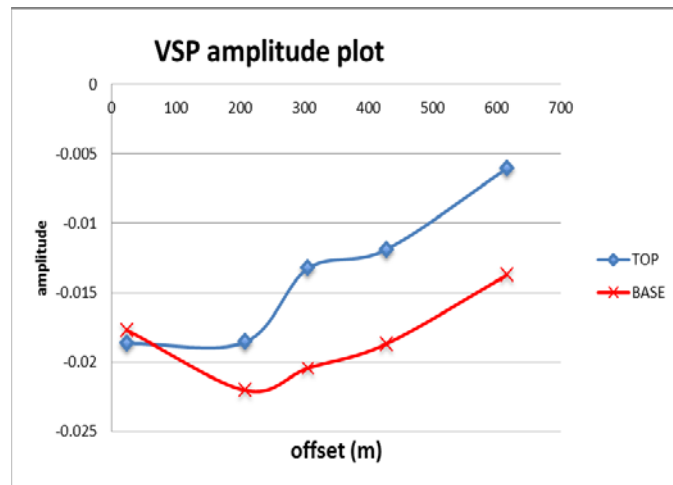


FIG. 22. An amplitude vs offset plot of horizons picked from VSP gather. The red line is amplitude of the top reservoir and the blue line is the amplitude of the reservoir bottom.

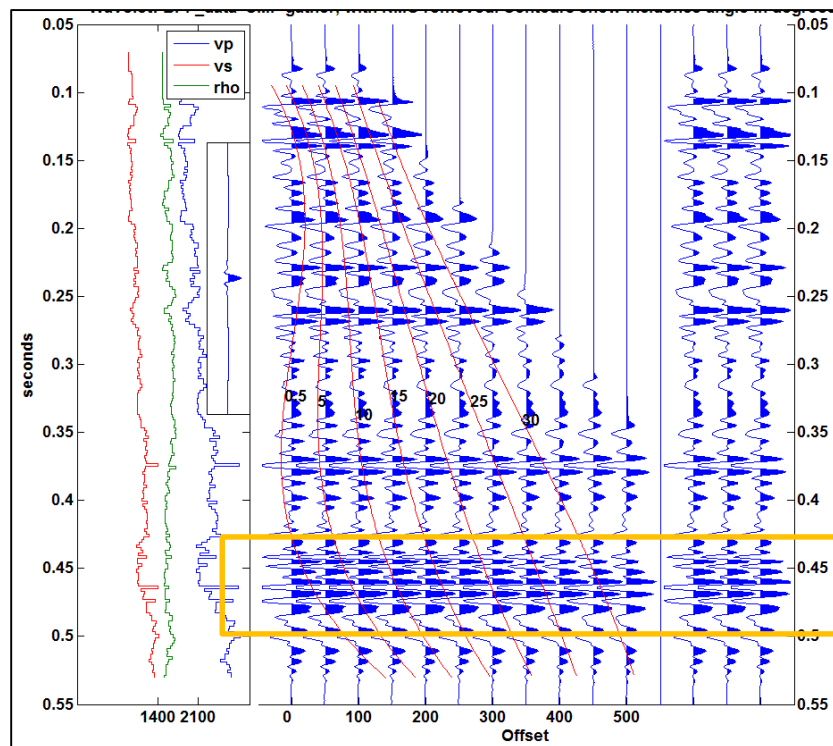


FIG. 23. Synthetic P-P CMP gather and its stacked trace (repeated 3 times). Contours show the incident angles. The target zone is highlighted by the yellow rectangle.

Table 4. Amplitudes picked from the synthetic gather.

TRACE NO.	OFFSET	TOP	A	BASE	B
1	0	-0.054	0.153	-0.136	0.022
2	50	-0.053	0.153	-0.135	0.022
3	100	-0.052	0.151	-0.132	0.021
4	150	-0.049	0.149	-0.129	0.020
5	200	-0.047	0.147	-0.123	0.018
6	250	-0.043	0.144	-0.117	0.014
7	300	-0.040	0.137	-0.111	0.012
8	350	-0.036	0.132	-0.107	0.008
9	400	-0.031	0.126	-0.098	0.007
10	450	-0.027	0.116	-0.094	0.006
11	500	-0.024	0.108	-0.092	0.003

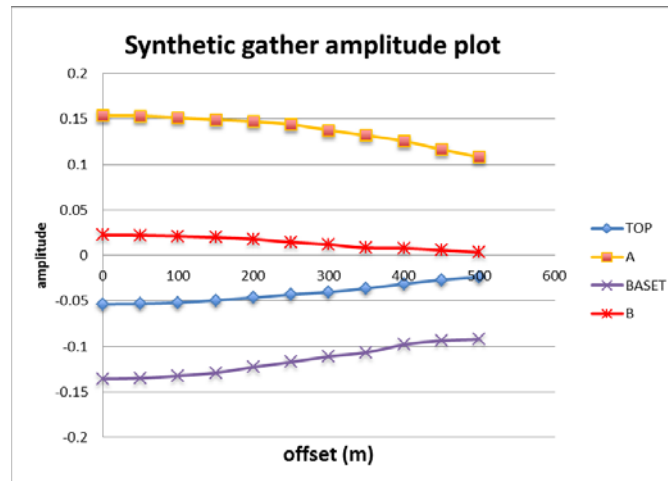


FIG. 24. The amplitude vs offset plot of horizons picked from the synthetic gather in the target reservoir.

For better comparison, the amplitudes of top and bottom of the reservoir picked from VSP data were scaled to those picked from synthetic seismograms and were plotted in the same coordinates (FIG. 25). In FIG. 25, the left picture is an amplitude comparison of the top of the reservoir and right one is the comparison of the base of the reservoir. Overall, the amplitudes picked from VSP and synthetic seismogram at top and bottom of the reservoir display a similar variation trend within offset range of 0 to 500 m. These results give promise of rock properties inversion using the walkaway VSP.

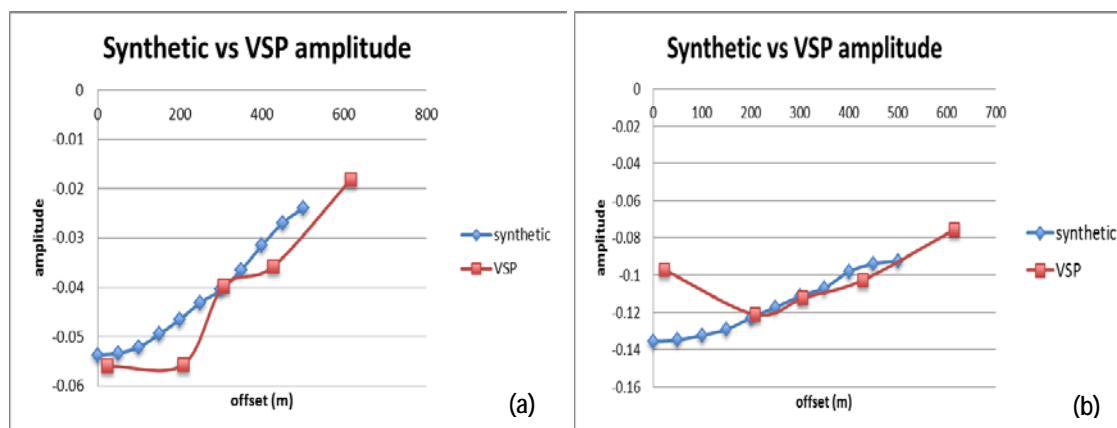


FIG. 25. Comparison of amplitudes picked from VSP and synthetic seismogram. (a) amplitude response of top reservoir; (b) amplitude response of base reservoir. In both the response shows similar trends along offset.

SUMMARY AND FUTURE WORK

A multicomponent walkaway VSP data was processed and correlated to synthetic seismograms. Overall, the PP mode of VSP data shows good consistency with synthetic seismograms. Inside the reservoir, difference was observed due to production. The distance between analyzed well location and the VSP borehole may also degrade the accuracy of the interpretation. The PP wave AVO responses of VSP gather and synthetic seismogram show similar trends at the top and bottom of the reservoir. The results give us promise for rock properties inversion by the walkaway VSP data.

Future work in this research will be 1) obtain a more accurate PS wave velocity to process and correlate the PS data to PP data; 2) then undertake PP-PS joint inversion to predict the rock properties such as P and shear wave velocity, porosity, fluid factor etc.

ACKNOWLEDGEMENTS

We thank an unidentified company for providing the VSP data for this research and for permission to publish the results. We also thank GEDCO/Schlumberger for providing the VISTA software and technical support during the data processing. Finally, we give thanks to all of the CREWES sponsors for support of this research. We also gratefully acknowledge support from NSERC (Natural Science and Engineering Research Council of Canada) through the grant CRDPJ 379744-08.

REFERENCE

- Bubshait, S., 2010, VSP processing for coal reflections, M.Sc. Thesis, Department of Geoscience, University of Calgary.
- Coulombe, C.A., Stewart, R.R., and Jones, M.J., 1996, AVO processing and interpretation of VSP data, Canadian Journal of Exploration Geophysics, Volume 32, 41-62.
- Hall, K. W., Lawton, D. C., Holloway, D., and Gallant, E.V., 2012, Walkaway 3C-VSP, CREWES Research Report, Volume 24.

- Hardage, B. A., 1983, Vertical seismic profiling-principles (1st ed.): Amsterdam, Geophysical Press, 470p.
- Hein, F., Weiss, J., and Berhane, H., 2007, Cold Lake Oil Sands Area: Formation Picks and Correlation of Associated Stratigraphy, The Alberta Energy and Utilities Board/ Alberta Geological Survey (EUB/AGS) Geo-Note, 2006-03
- Hinds, R.C., Kuzmiski, R.D., Botha, W.J., and Anderson, N.L., 1989, Vertical and lateral seismic profile, in Anderson N.L., Hills, L.V. and Cederwall, D.A., Eds., Geophysical Atlas of Western Canadian Hydrocarbon Pools, CSEG/CSPG, 319-344
- Hinds, R.C., Anderson, N.L., and Kuzmiski, R.D., 2007, VSP interpretative processing: Theory and practice, SEG Continuing Education Course Notes.
- Hinds, R.C., and Kuzmiski, R.D., 2001, VSP for the interpreter/processor for 2001 and beyond: part1, CSEG Recorder, Volume **26**, No.9, 84-95.
- Lawton, D.C, Gary, M. F., and Stewart, R. R., 2012, Reflections on PS: An interactive discussion of problems and promise in converted-wave exploration, CREWES Research Report, Volume **24**.
- Lines, L.R., and Newrick, R.T., 2004, Fundamentals of geophysical interpretation, Geophysical Monograph Series, Number 13, Society Of Exploration Geophysicists.
- Margrave, G.F., 2008, Methods of seismic data processing, Geophysics 557 Course Lecture Notes, Department of Geology and Geophysics, University of Calgary.
- Wiggins, J.W., Ng, P., and Mazur, A., 1986, The relation between the VSP-CDP transformation and VSP migration: 55th Ann. Internat. Mtg., SEG Expanded Abstract.
- Xu, C., and Stewart, R. R., Ross Lake 3C-3D seismic survey and VSP, Saskatchewan: A preliminary interpretation, 2003, CREWES Research Report, Volume **15**.